Heliyon

ELSEVIER

Received:
29 March 2016
Revised:
21 June 2016
Accepted:
5 August 2016

Heliyon 2 (2016) e00140

Finite element analysis of double-diffusive natural convection in a porous triangular enclosure filled with Al_2O_3-water nanofluid in presence of heat generation

Raju Chowdhury [a,b,*], **Salma Parvin** [b], **Md. Abdul Hakim Khan** [b]

[a] *Department of Natural Science, Stamford University Bangladesh, Dhaka 1217, Bangladesh*

[b] *Department of Mathematics, Bangladesh University of Engineering and Technology, Dhaka 1000, Bangladesh*

* Corresponding author at: Department of Natural Science, Room #A/119, Stamford University Bangladesh, 51, Siddeswari Road, Dhaka 1217, Bangladesh.

E-mail address: raju_chy_23@yahoo.com (R. Chowdhury).

Abstract

The problem of double-diffusive natural convection of Al_2O_3-water nanofluid in a porous triangular enclosure in presence of heat generation has been studied numerically in this paper. The bottom wall of the cavity is heated isothermally, the left inclined wall is non-isothermal and the right inclined wall is considered to be cold. The concentration is higher at bottom wall, lower at right inclined wall and non-isoconcentration at left inclined wall of the cavity. The governing equations are transformed to the dimensionless form and solved numerically using Galerkin weighted residual technique of finite element method. The results are obtained in terms of streamlines, isotherms, isoconcentrations, average Nueeslt number (Nu) and average Sherwood number (Sh) for the parameters thermal Rayleigh number (Ra_T), dimensionless heat generation parameter (λ), solid volume fraction (ϕ) and Lewis number (Le) while Prandtl number (Pr), Buoyancy ratio (N) and Darcy number (Da) are considered to be fixed. It is observed that flow pattern, temperature fields and concentration fields are affected by the variation of above considered parameters.

http://dx.doi.org/10.1016/j.heliyon.2016.e00140

Keywords: Computational mathematics, Engineering and thermodynamics

1. Introduction

Double-diffusive natural convection is very important topic to the researchers because of its variety application areas in engineering such as in heat exchanger devices, design of electronic equipment, petroleum reservoirs, insulation systems and solar collectors that are widely reviewed by Nield and Bejan [1] and Ingham and Pop [2].

Enhancement of heat transfer in cavities becomes burning issues from industrial and energy perspectives. In the past few years, experimentally, analytically and numerically extensive researches have been performed by many researchers to improve the heat transfer in cavities [3, 4, 5, 6, 7, 8, 9]. Fluid that have been generally used for heat transfer applications, such as water, mineral oils, and ethylene glycol, is failure to meet the growing demand as an efficient heat transfer agent. To fulfill the rising demand of modern technology, for instance chemical production, power stations and micro-electronics, it is necessary to develop such types of fluids that will perform more effectively in case of heat exchange. Such new types of fluid are nanofluids, which are new heat transfer fluids containing a small quantity of nanosized particles suspended in a base fluid. These nanofluids have very high thermal conductivity and many researchers [9, 10] have investigated that by adding nanoparticle with low volume fraction (1–5%) in the base fluid, the thermal conductivity can be increased by about 20%.

Natural convective heat transfer with heat generation effect has received significant amount of attention for extensive engineering applications in geophysics and energy related fields. Acharya and Goldstein [11] have studied natural convection in an externally heated complicated cavity with internal heat generation. Natural convection and entropy generation of nanofluid filled cavity having different shaped obstacles under the influence of magnetic field and internal heat generation has been invested by Selimefendigil and Oztop [12]. Chowdhury et al. [13] have analyzed MHD natural convection in a porous equilateral triangular enclosure with a heated square body in the presence of heat generation. Selimefendigil and Oztop [14] have studied mixed convection in a two-sided elastic walled and SiO_2 nanofluid filled cavity with internal heat generation: effects of inner rotating cylinder and nanoparticle's shape.

Double-diffusive convection is a fluid dynamics topic that describes a form of convection driven by two different density gradients, which have different rates of diffusion [15, 16, 17]. Combined heat and mass transfer occurs in a wide range of applications in both nature and industry. In nature, such flows are occurred in oceans, lakes, and the atmosphere. In industry, these types of flows are the chemical process, solidification, food processing and migration of impurities in

http://dx.doi.org/10.1016/j.heliyon.2016.e00140

non-isothermal material processing applications. Ostrach [18] and Viskanta et al. [19] have reported complete reviews on the subject. Natural convection in rectangular porous enclosures due to constant fluxes of heat and mass on the vertical walls has been investigated by Alavyoon [20]. Mamou et al. [21] have studied numerically double-diffusion convection in an inclined slot porous enclosure. Double diffusive natural convective heat transfer flows in a square enclosure have been investigated by Esfahani and Bordbar [22]. They have used water base nanofluids as a working fluid. Teamah et al. [23] have done numerical simulation on double diffusive natural convection flow in an inclined rectangular cavity considering both magnetic field and heat source. Bejan [24] has conducted natural convective mass and heat transfer flow in a vertical enclosure. An experimental work has examined by Kamotani [25] on natural convection in a shallow enclosures with horizontal temperature and concentration gradients. Mamou et al. [26] have studied numerically double-diffusive convection in an inclined porous enclosure using Galerkin finite element formulations.

A porous medium is characterized by a partitioning of the total volume into solid matrix and pore space, with the latter being filled by one or more fluids. Double-diffusive natural convection in a porous media has many engineering and geophysical applications such as geothermal reservoirs, drying of porous solids, thermal insulation, enhanced oil recovery and packed bed catalytic reactors. Combined heat and mass transfer in a porous triangular enclosure can be a simple model for many engineering applications such as insulation for buildings, nuclear waste management and heat exchangers. Although many studies have reported natural convection in triangular cavities [27], studies in combined heat and mass transfer in triangular enclosures filled with Al_2O_3-water nanofluid are very limited. The aim of the present study is to investigate the flow pattern, heat and mass transfer phenomenon in a porous triangular enclosure filled with Al_2O_3-water nanofluid exposed to both temperature and concentration gradients. The flow is assumed to operate in the laminar regime under steady state conditions. Double-diffusive conditions is maintained by taking the bottom wall as heated wall and the source for solute concentration as well, the right inclined wall is cold and lower concentration and the left inclined wall is non-isothermal and non-isoconcentration. To predict the ratio of thermal conductivity restricted to spherical nanoparticles, the Maxwell-Garnett (MG) model has been used.

2. Model

Fig. 1 shows the schematic diagram of triangular enclosure subjected to the boundary conditions. The bottom wall of the cavity is heated uniformly at temperature T_h, the left inclined wall is non-isothermal and the right inclined wall is considered to be cold at temperature T_c. The concentration, c_h is higher at bottom wall, lower c_c at right inclined wall and non-isoconcentration at left

http://dx.doi.org/10.1016/j.heliyon.2016.e00140

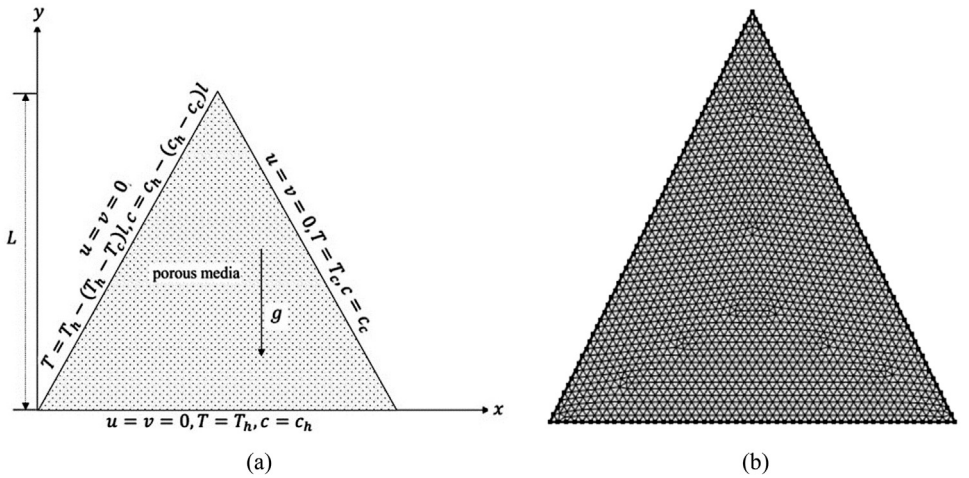

Fig. 1. (a) Physical model of the problem with corresponding boundary conditions and (b) Mesh structure of elements for triangular enclosure.

inclined wall of the cavity. The working fluid considered in the system is a water based Al_2O_3 nanofluid. The symbols used here are defined in Table 1 and the properties of water and Al_2O_3 are presented in Table 2. The physical properties of the fluid are assumed to be constant except the density in the buoyancy force term.

Table 1. Nomenclature.

c	concentration $[mol\ m^{-3}]$	α	thermal diffusivity $\left[ms^{-2}\right]$
C	dimensionless concentration	β_T	volumetric coefficient of thermal expansion $\left[K^{-1}\right]$
C_p	specific heat $\left[J\,kg^{-1}\,K^{-1}\right]$	β_s	volumetric coefficient of solutal expansion $\left[m^3kg^{-1}\right]$
D	mass diffusivity $[m^2/s]$	λ	dimensionless heat generation parameter
g	gravity acceleration $\left[m/s^2\right]$	μ	dynamic viscosity $[kg\ m^{-1}s^{-1}]$
k	thermal conductivity $\left[Wm^{-1}\,K^{-1}\right]$	θ	dimensionless temperature
l	length of the inclined wall $[m]$	ν	kinematic viscosity $\left[m^2s^{-1}\right]$
L	height of the triangle $[m]$	ρ	density $\left[kg\,m^{-3}\right]$
N	buoyancy ratio, $\beta_s\nabla_c/\beta_T\nabla T$	ϕ	nanoparticle volume fraction
p	fluid pressure$[Pa]$	ℓ	dimensionless length of inclined wall
P	dimensionless fluid pressure		
$u,\ v$	$x,\ y$ component of velocity $\left[ms^{-1}\right]$	c	cold
$U,\ V$	$x,\ y$ component of dimensionless velocity	h	hot
T	Temperature $[K]$	f	fluid
		p	nanoparticle
		nf	nanofluid

http://dx.doi.org/10.1016/j.heliyon.2016.e00140

The steady two dimensional governing equations of conservation of mass, momentum, energy and concentration used for nanofluids can be written as:

$$\frac{\partial u}{\partial x}+\frac{\partial v}{\partial y}=0 \tag{1}$$

$$\rho_{nf}\left(u\frac{\partial u}{\partial x}+v\frac{\partial u}{\partial y}\right)=-\frac{\partial p}{\partial x}+\mu_{nf}\left(\frac{\partial^2 u}{\partial x^2}+\frac{\partial^2 u}{\partial y^2}\right)-\frac{\mu_{nf}}{K}u \tag{2}$$

$$\begin{aligned}\rho_{nf}\left(u\frac{\partial v}{\partial x}+v\frac{\partial v}{\partial y}\right)&=-\frac{\partial p}{\partial y}+\mu_{nf}\left(\frac{\partial^2 v}{\partial x^2}+\frac{\partial^2 v}{\partial y^2}\right)-\frac{\mu_{nf}}{K}v\\&\quad+\rho_{nf}g[\beta_T(T-T_c)+\beta_s(c-c_c)]\end{aligned} \tag{3}$$

$$\left(u\frac{\partial T}{\partial x}+v\frac{\partial T}{\partial y}\right)=\alpha_{nf}\left(\frac{\partial^2 T}{\partial x^2}+\frac{\partial^2 T}{\partial y^2}\right)+\frac{Q_o}{(C_p)_{nf}}(T-T_c) \tag{4}$$

$$\left(u\frac{\partial c}{\partial x}+v\frac{\partial c}{\partial y}\right)=D_f\left(\frac{\partial^2 c}{\partial x^2}+\frac{\partial^2 c}{\partial y^2}\right) \tag{5}$$

The boundary conditions of the above equations are:

On the left wall: $u=v=0, T=T_h-(T_h-T_c)l, c=c_h-(c_h-c_c)l$

On the right wall: $u=v=0, T=T_c, c=c_c$

On the bottom wall: $u=v=0, T=T_h, c=c_h$

Using the following dimensionless variables:

$$X=\frac{x}{L}, Y=\frac{y}{L}, U=\frac{uL}{\alpha_f}, V=\frac{vL}{\alpha_f}, \theta=\frac{T-T_c}{T_h-T_c}, C=\frac{c-c_c}{c_h-c_c}, P=\frac{pL^2}{\alpha_f^2}, \ell=\frac{l}{L} \tag{6}$$

The governing equations in non-dimensional form:

$$\frac{\partial U}{\partial X}+\frac{\partial V}{\partial Y}=0 \tag{7}$$

$$\left(U\frac{\partial U}{\partial X}+V\frac{\partial V}{\partial Y}\right)=-\frac{\partial P}{\partial X}+\frac{\mu_{nf}}{\rho_{nf}\alpha_f}\left(\frac{\partial^2 U}{\partial X^2}+\frac{\partial^2 U}{\partial Y^2}\right)-\frac{\mu_{nf}}{\rho_{nf}\alpha_f}\frac{1}{Da}U \tag{8}$$

$$\left(U\frac{\partial V}{\partial X}+V\frac{\partial V}{\partial Y}\right)=-\frac{\partial P}{\partial Y}+\frac{\mu_{nf}}{\rho_{nf}\alpha_f}\left(\frac{\partial^2 V}{\partial X^2}+\frac{\partial^2 V}{\partial Y^2}\right)-\frac{\mu_{nf}}{\rho_{nf}\alpha_f}\frac{1}{Da}V+Ra_T\mathbf{Pr}(\theta+NC) \tag{9}$$

Table 2. Thermophysical properties of water and nanoparticles.

Physical Properties	$C_{p(J/KgK)}$	$\rho(kg/m^3)$	k (W/mK)	$\beta_{(1/K)}$
Water	4179	997.1	0.613	21×10^{-5}
Al_2O_3	765	3970	40	0.8×10^{-5}

http://dx.doi.org/10.1016/j.heliyon.2016.e00140

$$\left(U\frac{\partial \boldsymbol{\theta}}{\partial X}+V\frac{\partial \boldsymbol{\theta}}{\partial Y}\right)=\frac{\boldsymbol{\alpha}_{nf}}{\boldsymbol{\alpha}_f}\left(\frac{\partial^2 \boldsymbol{\theta}}{\partial X^2}+\frac{\partial^2 \boldsymbol{\theta}}{\partial Y^2}\right)+\boldsymbol{\lambda\theta} \tag{10}$$

$$\left(U\frac{\partial C}{\partial X}+V\frac{\partial C}{\partial Y}\right)=\frac{1}{Le}\left(\frac{\partial^2 C}{\partial X^2}+\frac{\partial^2 C}{\partial Y^2}\right) \tag{11}$$

where the thermal Rayleigh number $Ra_T=\dfrac{g\boldsymbol{\beta}_{ff}(T_h-T_c)L^3}{\boldsymbol{\alpha}_f\boldsymbol{\mu}_f}$, the solutal Rayleigh number $Ra_S=\dfrac{g\boldsymbol{\beta}_{Sf}(C_h-C_c)L^3}{\boldsymbol{\alpha}_f\boldsymbol{\mu}_f}$, Prandtl number $\Pr=\dfrac{\boldsymbol{\nu}_f}{\boldsymbol{\alpha}_f}$, Darcy number $Da=\dfrac{K}{L^2}$, heat generation parameter $\boldsymbol{\lambda}=\dfrac{Q_0L^2}{(C_p)_{nf}\boldsymbol{\alpha}_f}$, Buoyancy ratio $N=\dfrac{Ra_S}{Ra_T}$ and Lewis number $Le=\dfrac{\boldsymbol{\alpha}_f}{D_f}$.

The non-dimensional boundary conditions are:

On the right inclined wall: $U=V=0,\boldsymbol{\theta}=0,C=0$

On the left inclined wall: $U=V=0,\boldsymbol{\theta}=1-\ell,C=1-\ell$.

On the bottom wall: $U=V=0,\boldsymbol{\theta}=1,C=1$.

The effective thermal conductivity of the nanofluid is approximated by the Hamilton-Crosser model [28] expressed as

$$k_{nf}=k_f\frac{k_p+2k_f-2\boldsymbol{\phi}(k_f-k_p)}{k_p+2k_f-\boldsymbol{\phi}(k_f-k_p)}$$

The viscosity of the nanofluid is approximated by Brinkman [29]

$$\boldsymbol{\mu}_{nf}=\frac{\boldsymbol{\mu}_f}{(1-\boldsymbol{\phi})^{2.5}}$$

The volumetric coefficient of thermal expansion $(\boldsymbol{\beta}_T)_{nf}=(1-\boldsymbol{\phi})(\boldsymbol{\beta}_T)_f+\boldsymbol{\phi}(\boldsymbol{\beta}_T)_p$, density $_{nf}=(1-\boldsymbol{\phi})_f+\boldsymbol{\phi}_p$, thermal diffusivity $\boldsymbol{\alpha}_{nf}=\frac{k_{nf}}{(C_p)_{nf}}$, and heat capacitance $(C_p)_{nf}=(1-\boldsymbol{\phi})(C_p)_f+\boldsymbol{\phi}(C_p)_p$.

The local and average Nusselt number along the heated bottom wall can be calculated as

$$\boldsymbol{Nu_b}=-\frac{\boldsymbol{k_{nf}}}{\boldsymbol{k_f}}\left(\frac{\partial \boldsymbol{\theta}}{\partial \boldsymbol{n}}\right),\ Nu=-\left(\frac{k_{nf}}{k_f}\right)\frac{1}{L}\int_0^L\left(\frac{\partial \boldsymbol{\theta}}{\partial n}\right)dL \tag{12}$$

The local and average Sherwood number along the heated bottom wall are calculated as

$$\boldsymbol{Sh_b}=-\left(\frac{\partial C}{\partial n}\right),\ Sh=-\frac{1}{L}\int_0^L\left(\frac{\partial C}{\partial n}\right)dL \tag{13}$$

3. Methodology

3.1. Numerical method

Galerkin weighted residual method of finite element formulation has been used as numerical procedure in this study. Due to the mass conservation, the continuity equation has been considered as a constraint. The velocity components U, V, the temperature $\boldsymbol{\theta}$, the concentration C and the pressure P are the basic unknowns of the differential equations (8)–(11). It is assuming that the flow domain to be analyzed is divided into subdomains called finite element. Many types of element are encountered in finite element method. In two dimensional problems, commonly used elements are triangular and quadrilateral. The six node triangular element has been used in this study for the development of the finite element equations. All nodes are connected with velocities, temperature and concentration while the corner nodes are merely related with the pressure. Selection of interpolating functions is the critical step in finite element analysis. A lower order polynomial is chosen for pressure comparing the velocity field. The velocity component and the temperature distributions and linear interpolation for the pressure distribution according to their highest derivative orders in the differential equations (8)–(11) as

$$U(X,Y) = \Sigma N_\beta U_\beta,\ \ V(X,Y) = \Sigma N_\beta V_\beta,\ \ \theta(X,Y) = \Sigma N_\beta \theta_\beta,\ \ C(X,Y) = \Sigma N_\beta C_\beta,$$
$$P(X,Y) = \Sigma N_\beta P_\beta$$

Where $\boldsymbol{\beta} = 1, 2, \ldots .., 6; \boldsymbol{\mu} = 1, 2, 3.$

Substituting the element velocity component distributions, the temperature distribution, the concentration distribution and the pressure distribution from the equations (8)–(11), the finite element equations can be written in the form:

$$K_{\boldsymbol{\alpha\beta\alpha}^x} U_\beta U_{\boldsymbol{\alpha}} + K_{\boldsymbol{\alpha\beta\alpha}^y} V_\beta U_{\boldsymbol{\alpha}} + R_{\boldsymbol{\lambda\mu}^x} P_{\boldsymbol{\mu}} + \frac{\boldsymbol{\mu}_{nf}}{{}_{nf}\boldsymbol{\alpha}_f}\left(K_{\boldsymbol{\alpha\beta}^{xx}} + K_{\boldsymbol{\alpha\beta}^{yy}}\right) U_{\boldsymbol{\beta}} + \frac{\boldsymbol{\mu}_{nf}}{{}_{nf}\boldsymbol{\alpha}_f} K_{\boldsymbol{\alpha\beta}} U_{\boldsymbol{\beta}} = Q_{\boldsymbol{\alpha}^u} \tag{14}$$

$$K_{\alpha\beta\gamma^x} U_\beta V_\gamma + K_{\alpha\beta\gamma^y} V_\beta V_\gamma + R_{\lambda\mu^y} P_\mu + \frac{\mu_{nf}}{\rho_{nf}\alpha_f}\left(K_{\alpha\beta^{xx}} + K_{\alpha\beta^{yy}}\right) V_\beta + \frac{\mu_{nf}}{\rho_{nf}\alpha_f} K_{\alpha\beta} V_\beta - Ra_T Pr K_{\alpha\beta}\theta_\beta - Ra_T Pr N K_{\alpha\beta} C_\beta + Ha^2 K_{\alpha\beta} V_\beta = Q_{\alpha^v} \tag{15}$$

$$K_{\boldsymbol{\alpha\beta\alpha}^x} U_{\boldsymbol{\beta}} \boldsymbol{\theta}_{\boldsymbol{\alpha}} + K_{\boldsymbol{\alpha\beta\alpha}^y} V_{\boldsymbol{\beta}} \boldsymbol{\theta}_{\boldsymbol{\alpha}} + \frac{\boldsymbol{\alpha}_{nf}}{\boldsymbol{\alpha}_f}\left(K_{\boldsymbol{\alpha\beta}^{xx}} + K_{\boldsymbol{\alpha\beta}^{yy}}\right)\boldsymbol{\theta}_{\boldsymbol{\beta}} - \boldsymbol{\lambda} K_{\boldsymbol{\alpha\beta}} \boldsymbol{\theta}_{\boldsymbol{\beta}} = Q_{\boldsymbol{\alpha}^\theta} \tag{16}$$

$$K_{\boldsymbol{\alpha\beta\alpha}^x} U_{\boldsymbol{\beta}} C_{\boldsymbol{\alpha}} + K_{\boldsymbol{\alpha\beta\alpha}^y} V_{\boldsymbol{\beta}} C_{\boldsymbol{\alpha}} + \frac{1}{Le}\left(K_{\boldsymbol{\alpha\beta}^{xx}} + K_{\boldsymbol{\alpha\beta}^{yy}}\right) C_{\boldsymbol{\beta}} = Q_{\boldsymbol{\alpha}^C} \tag{17}$$

where the coefficients in element matrices are in the form of the integrals over the element area and along the element edges S_0 and S_w as

http://dx.doi.org/10.1016/j.heliyon.2016.e00140

$$K_{\alpha\beta} = \int N_\alpha N_\beta \, dA, \quad K_{\alpha\beta^x} = \int N_\alpha \frac{\partial N_\beta}{\partial X} dA, \quad K_{\alpha\beta^y} = \int N_\alpha \frac{\partial N_\beta}{\partial Y} dA,$$
$$K_{\alpha\beta^{xx}} = \int \frac{\partial N_\alpha}{\partial X} \frac{\partial N_\beta}{\partial X} dA, \quad K_{\alpha\beta^{xy}} = \int \frac{\partial N_\alpha}{\partial Y} \frac{\partial N_\beta}{\partial Y} dA, \quad K_{\alpha\beta\gamma^x} = \int N_\alpha N_\beta \frac{\partial N_\gamma}{\partial X} dA,$$
$$K_{\alpha\beta\gamma^y} = \int N_\alpha N_\beta \frac{\partial N_\gamma}{\partial Y} dA, \quad R_{\lambda\mu^x} = \int N_\lambda \frac{\partial N_\mu}{\partial X} dA, \quad R_{\lambda\mu^y} = \int N_\lambda \frac{\partial N_\mu}{\partial Y} dA,$$
$$Q_{\alpha^u} = \frac{\mu_{nf}}{\rho_{nf}\alpha_f} \int N_\alpha S_x ds_0, \quad Q_{\alpha^v} = \frac{\mu_{nf}}{\rho_{nf}\alpha_f} \int N_\alpha S_y ds_0, \quad Q_{\alpha^\theta} = \frac{\alpha_{nf}}{\alpha_f} \int N_\alpha q_\theta ds_w,$$
$$Q_{\alpha^c} = \frac{1}{Le} \int N_\alpha q_c ds_w.$$

The derived finite element equations (14)–(17) are system of nonlinear ordinary differential equations. These ordinary equations are solved by applying fourth order Runge-Kutta Method.

3.2. Validation

A test has been performed to valid the present study by comparing with earlier study Ahmed et al. [30]. Fig. 2 represents the results in terms of streamlines, isotherms and isoconcentrations obtained by the present code and the results

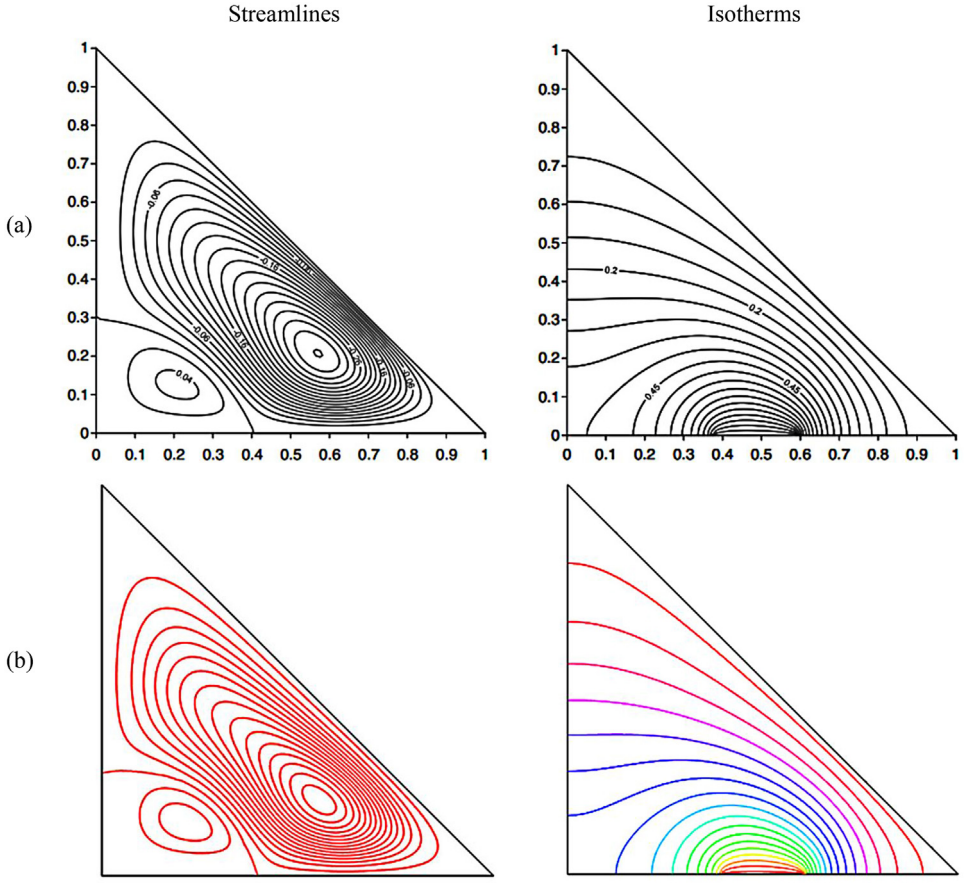

Fig. 2. A comparison for streamlines (left column) and isotherms (right column) between Ahmed et al. [30] (top row) and present study (bottom row) for $Ra = 10^4$, $Pr = 6.2$, $B = 0.2$, $\varphi = 5\%$, $D = 0.5$ and $Da = 10^{-3}$.

http://dx.doi.org/10.1016/j.heliyon.2016.e00140

presented by [30]. The comparison shows in Fig. 2 and it can be clearly seen that there is good agreement between the results.

3.3. Grid independence test

In the finite element formulation, the mesh generation is an approach in which a domain is subdivided into a set of subdomains, called finite elements. The discrete locations are defined by the numerical grid, at which the variables are to be calculated. It is basically a discrete representation of the geometric domain on which the problem is to be solved. Mesh generation of elements for the considered cavity is shown in Fig. 1(b). To determine the proper grid size for this study, a grid independence test is conducted with four types of mesh for $Pr = 7.0, Ra = 10^5, N = 1, Le = 1, Da = 10^{-3}$ and $\lambda = 0$ which are shown in Table 3. The extreme values of average Nusselt number (Nu) and average Sherwood number (Sh) are used as the sensitivity measure of the accuracy of the solution and are selected as the monitoring variable. Considering both the accuracy of numerical values and computational time, the present calculations are performed with 7,111 nodes and 13,736 elements grid system.

4. Results and discussion

The natural convection inside a porous triangular cavity filled with nanofluid with heat generation effect is influenced by the controlling parameters $10^4 \leq Ra_T \leq 10^6, 0 \leq \lambda \leq 10, 1 \leq Le \leq 10$ and $0 \leq \phi \leq 20$. The results are represented in terms of streamlines, isotherms, isoconcentration, average Nusselt number (Nu) and average Sherwood number (Sh) for parameters Ra_T, λ, ϕ and Le varied while $Pr=7.0, N=1, Da=10^{-3}$ are kept fixed.

Fig. 3 represents streamlines for different values of Ra_T and heat generation parameter λ while $Pr = 7.0, \phi = 10\%, Le = 1, N = 1, Da = 10^{-3}$. It can be shown that a triangular shape clockwise flow are formed within the cavity for $\lambda = 0$ and $Ra_T = 10^4$, the flow moves upwards near the heated wall and downwards near the cold wall. This is due to the fact that for lower values of thermal Rayleigh number

Table 3. Grid sensitivity check at $Pr = 7.0, Ra = 10^5, N = 1, Le = 1, Da = 10^{-3}$ and $\lambda = 0$.

Nodes	1783	3819	7111	8907
(elements)	(3613)	(6387)	(13736)	(17328)
Nu	10.5404	10.9382	11.2387	11.2387
Sh	8.5366	8.8831	9.1025	9.1025
Time (s)	145	179	212	268

http://dx.doi.org/10.1016/j.heliyon.2016.e00140

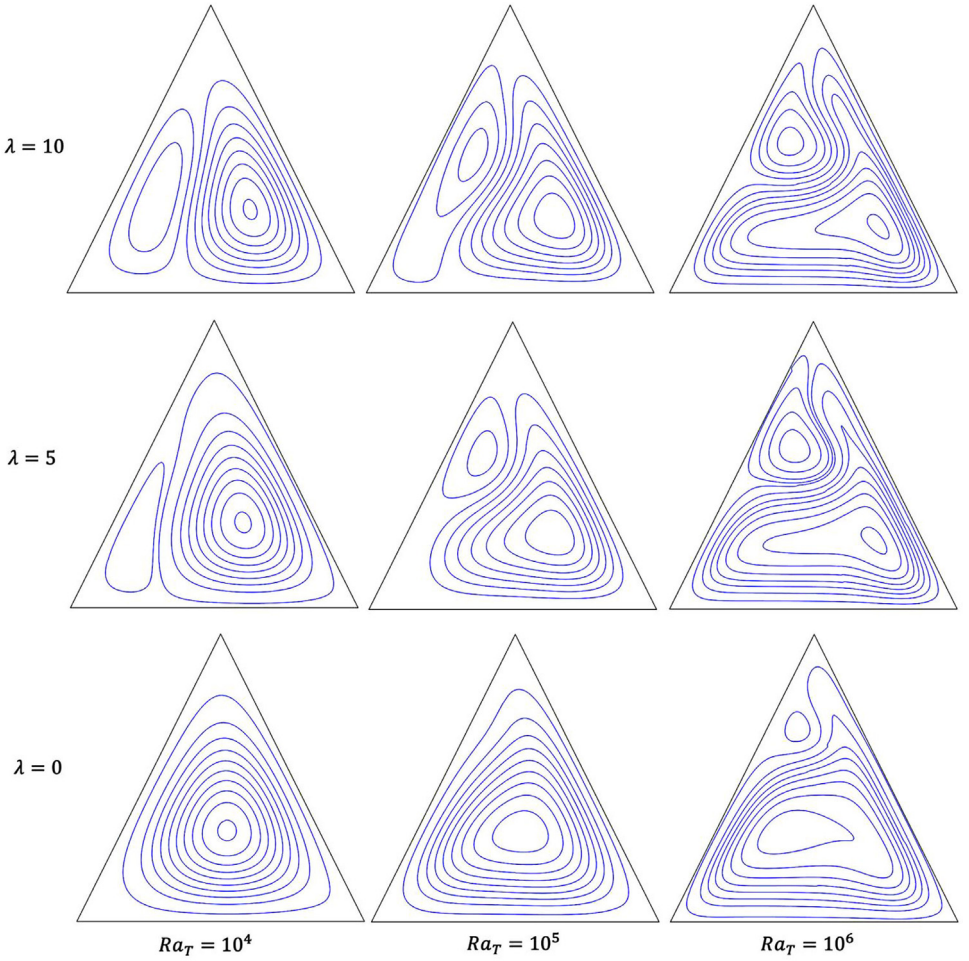

Fig. 3. Streamlines for different values of Ra_T and heat generation parameter λ with $Pr = 7.0$, $\varphi = 10\%$, $Le = 1$, $N = 1$, $Da = 10^{-3}$.

the conduction regime is dominant. For $Ra_T = 10^4$, and for all values of λ a secondary vortex is created at the left inclined wall of the cavity and the size of secondary vortex increases and occupies the space of the cavity due to increasing heat generation. The warm fluids discharge the temperature and the cold fluids near the right inclined wall receive that temperature. As a result, a clockwise fluid circulation occurred. With the increase of heat generation, the cold fluid receives the maximum temperature and fails to take any more temperature and thus an anticlockwise fluid re-circulation occurs. The similar result can be shown for $Ra_T = 10^5$ and $Ra_T = 10^6$ except the position of secondary vortex that takes place at the left upper corner of the cavity instead of left inclined wall for $Ra_T = 10^6$. This is because, with the increase of thermal Rayleigh number buoyant force becomes dominant and fluid velocity increases within the cavity.

http://dx.doi.org/10.1016/j.heliyon.2016.e00140

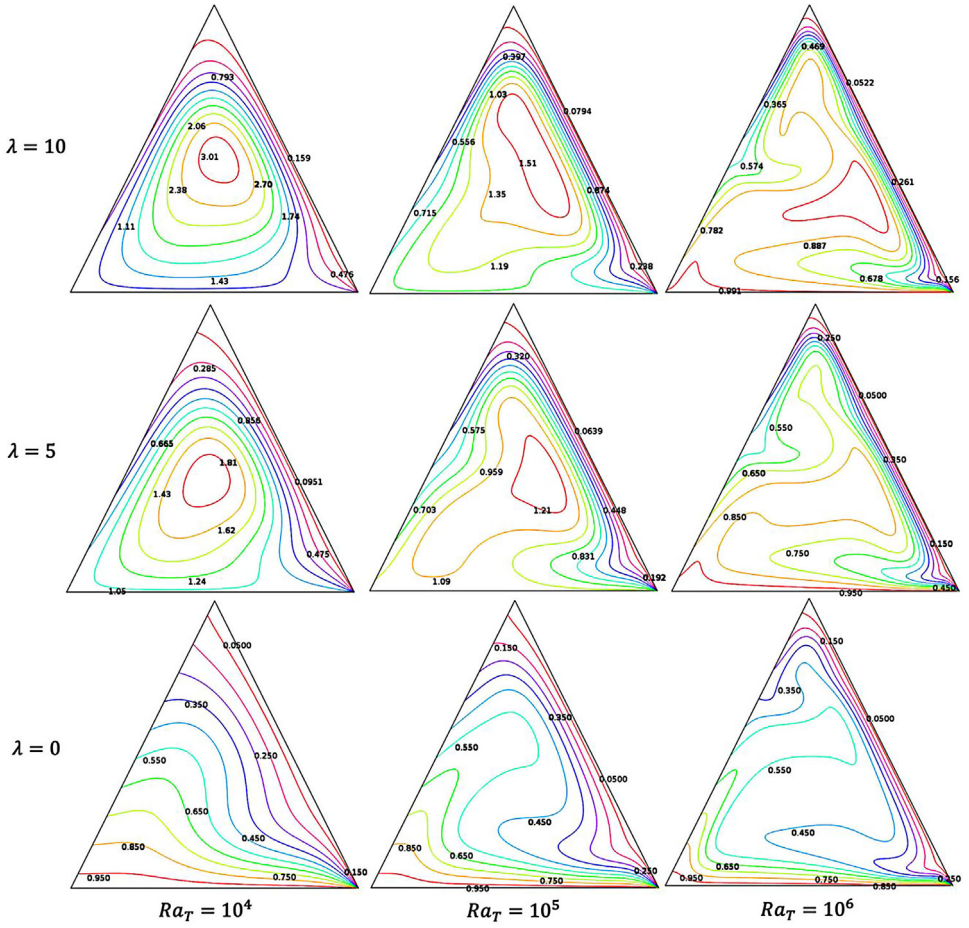

Fig. 4. Isotherms for different values of Ra_T and heat generation parameter λ with $Pr = 7.0$, $\varphi = 10\%$, $Le = 1$, $N = 1$, $Da = 10^{-3}$.

Fig. 4 and Fig. 5 describe the isotherms and isoconcentrations for different values of Ra_T and heat generation parameter λ. In Fig. 4, for $\lambda = 0$ and $Ra_T = 10^4$, isotherms looks like parallel near the bottom wall of the cavity. This happens since the bottom surface is heated constantly and heated boundary layer is developed adjacent to the bottom wall. Due to the buoyancy effect, the warm fluid within the boundary layer moves upward direction from the bottom left tip. With the increasing of heat generation the temperature gradient in the middle of the cavity also appears to increase. The temperature flows clockwise and moves towards the cold wall and becomes more clustered near the right inclined wall of the cavity for increasing Ra_T. This happens due to increasing buoyancy forces that causes natural convection in the cavity with the increasing of Rayleigh number. Fig. 5 shows the mass transport phenomenon with the increase of heat generation and Rayleigh number. From the figure, it can be clearly seen that the solutal gradient moves from

http://dx.doi.org/10.1016/j.heliyon.2016.e00140

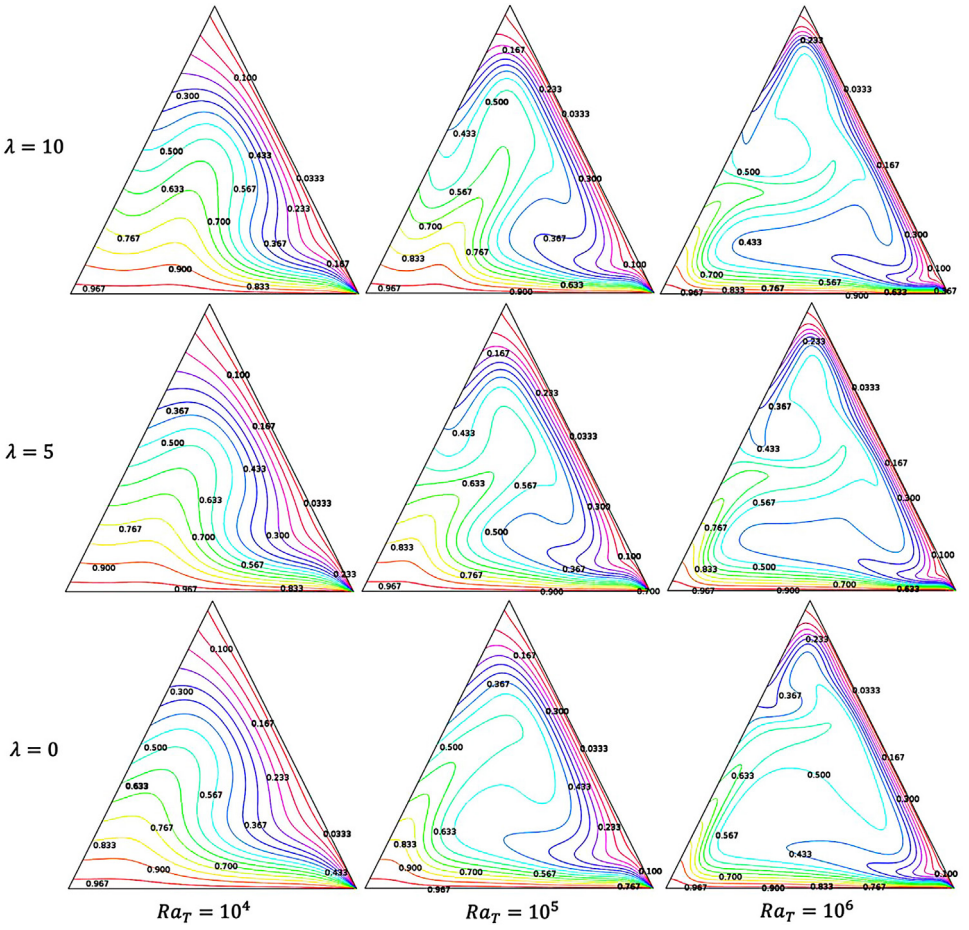

Fig. 5. Isoconcentrations for different values of Ra_T and heat generation parameter λ with $Pr = 7.0$, $\varphi = 10\%$, $Le = 1$, $N = 1$, $Da = 10^{-3}$.

the high concentration region to low concentration region for increasing both λ and Ra_T.

Fig. 6, Fig. 7, and Fig. 8 represent the flow strength, heat transport and species transport profile respectively for different values of Lewis number varies from 1 to 10 and Rayleigh number varies from 10^4 to 10^6 where $\mathrm{Pr} = 7.0, \boldsymbol{\phi} = 10\%, N = 1, \boldsymbol{\lambda} = 0$ and $Da = 10^{-3}$ are considered fixed. As the Lewis number represents the measure of thermal diffusivity to mass diffusivity of a fluid so, the larger value of Lewis number represents relatively low mass diffusivity value. Streamlines are almost similar for all values of Lewis number that can be seen in Fig. 6. From the figure it is clear that the strength of fluid flow is decreased with the increase of Lewis number. Comparing Fig. 7 and Fig. 8, it can be noticed that for increasing the Lewis number, the thickness of the solutal boundary layer near the heated bottom wall become thinner than thermal boundary layer. This means that the

http://dx.doi.org/10.1016/j.heliyon.2016.e00140

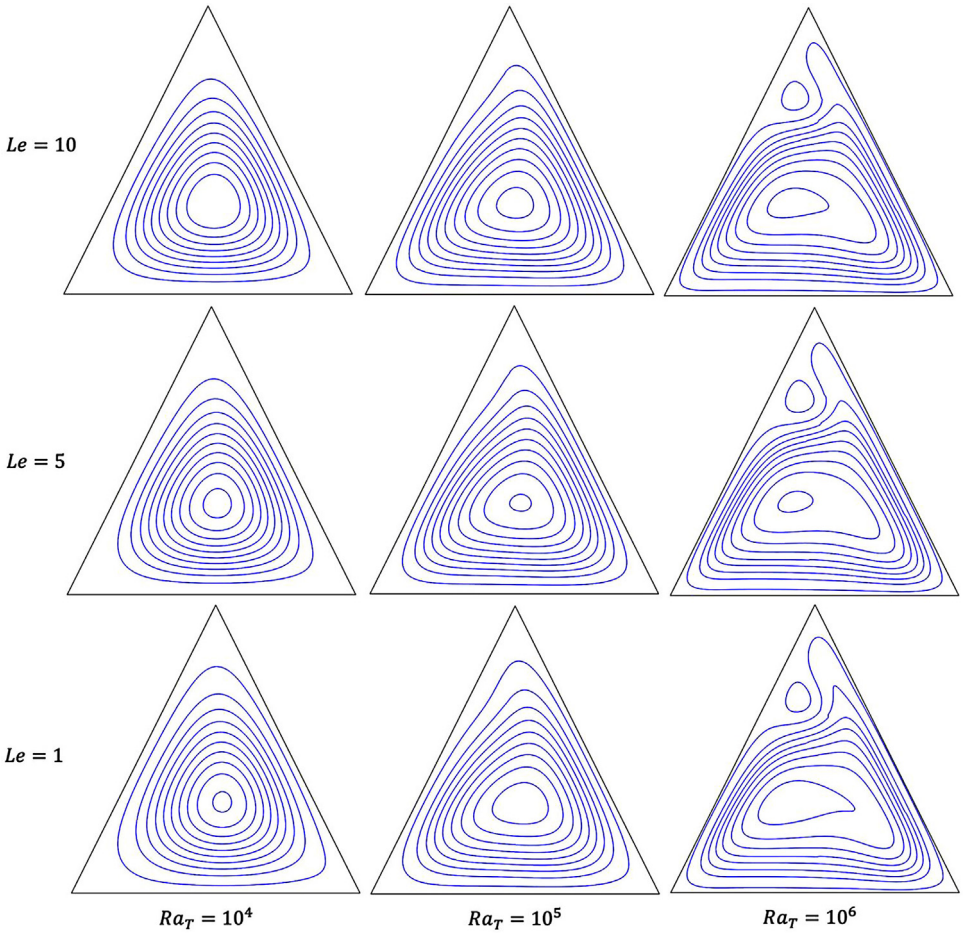

Fig. 6. Streamlines for different values of Ra_T and Le with $Pr = 7.0$, $\varphi = 10\%$, $\lambda = 0$, $N = 1$, $Da = 10^{-3}$.

thermal resistance is higher than the solutal resistance and therefore the mass transfer rate is higher than the heat transfer rate.

Fig. 9, Fig. 10 and Fig. 11 describe the investigation of the effect of dimensionless heat generation parameter, Lewis number and solid volume fraction on the heat and mass transfer rate on the bottom wall which is heated uniformly for different values of thermal Rayleigh number. The average Nusselt numbers and average Sherwood numbers are represented in Fig. 9 (a), (b) and the graph (a) demonstrate that the Nusselt number on the heated bottom wall increase with the increase of Rayleigh number and without heat generation whereas Nu reduce considerably with the increase of λ but Nu increase again at $Ra_T = 10^6$. This happens because the heat generation mechanism develops a boundary layer of hot fluid near the heated wall. As a result, the increasing rate of internal heat generation negates the heat transfer from the heated surface. The graph (b) demonstrate that the Sherwood number on

http://dx.doi.org/10.1016/j.heliyon.2016.e00140

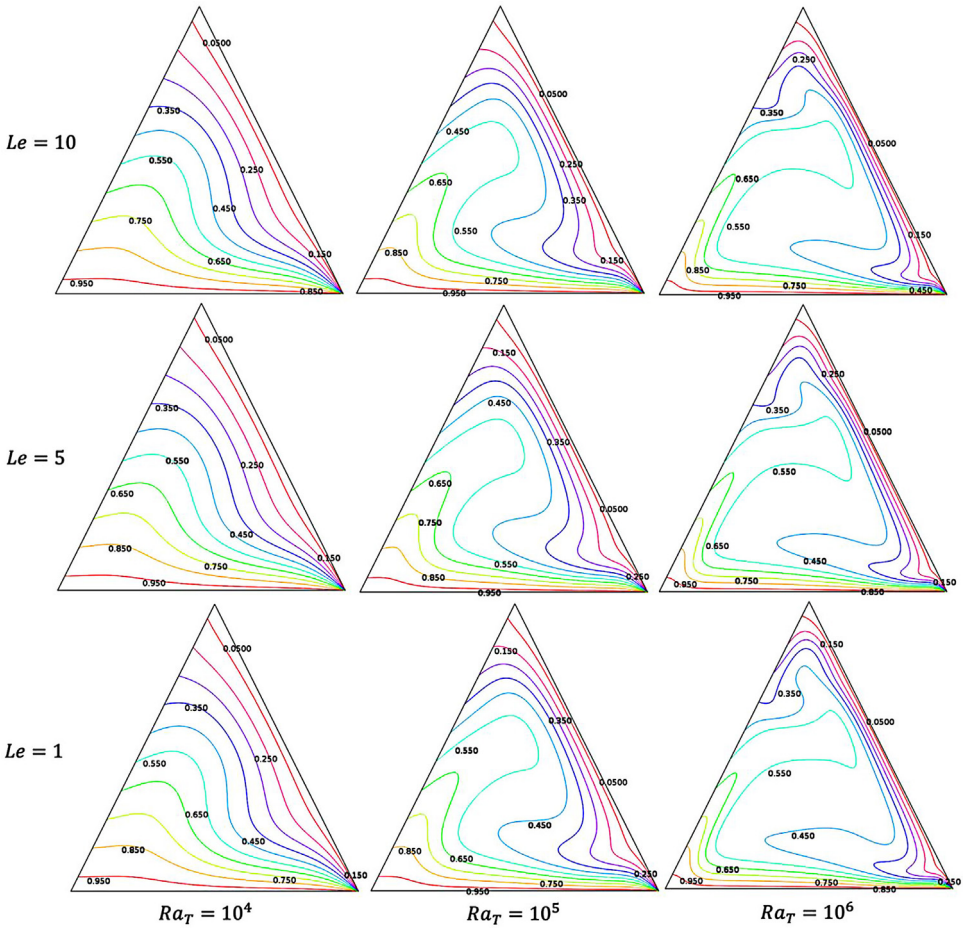

Fig. 7. Isotherms for different values of Ra_T and Le with $Pr = 7.0$, $\varphi = 10\%$, $\lambda = 0$, $N = 1$, $Da = 10^{-3}$.

the heated bottom wall increase with the increase of Ra_T and slightly decrease with the raising of λ.

The graphs from Fig. 10 (a),(b) demonstrate that the Nusselt number on the heated bottom wall reduce slightly while the Sherwood number rise up remarkably with the increase of Lewis number. From the figure, it can be inferred that both *Nu* and *Sh* are increased considerably when the thermal Rayleigh number is varied from 10^4 to 10^6 and mass transfer rate becomes decrease at $Ra_T = 10^6$.

Fig. 11 represents the average Nusselt number and average Sherwood number on the heated bottom wall for different values of thermal Rayleigh number and (Ra_T) solid volume fraction (ϕ). Increase of volume fraction of nanoparticles into the base fluid means the reduction of buoyancy, flow intensity and fluid temperature. As a result, the rate of heat transfer increases with the rise of volume fraction

http://dx.doi.org/10.1016/j.heliyon.2016.e00140

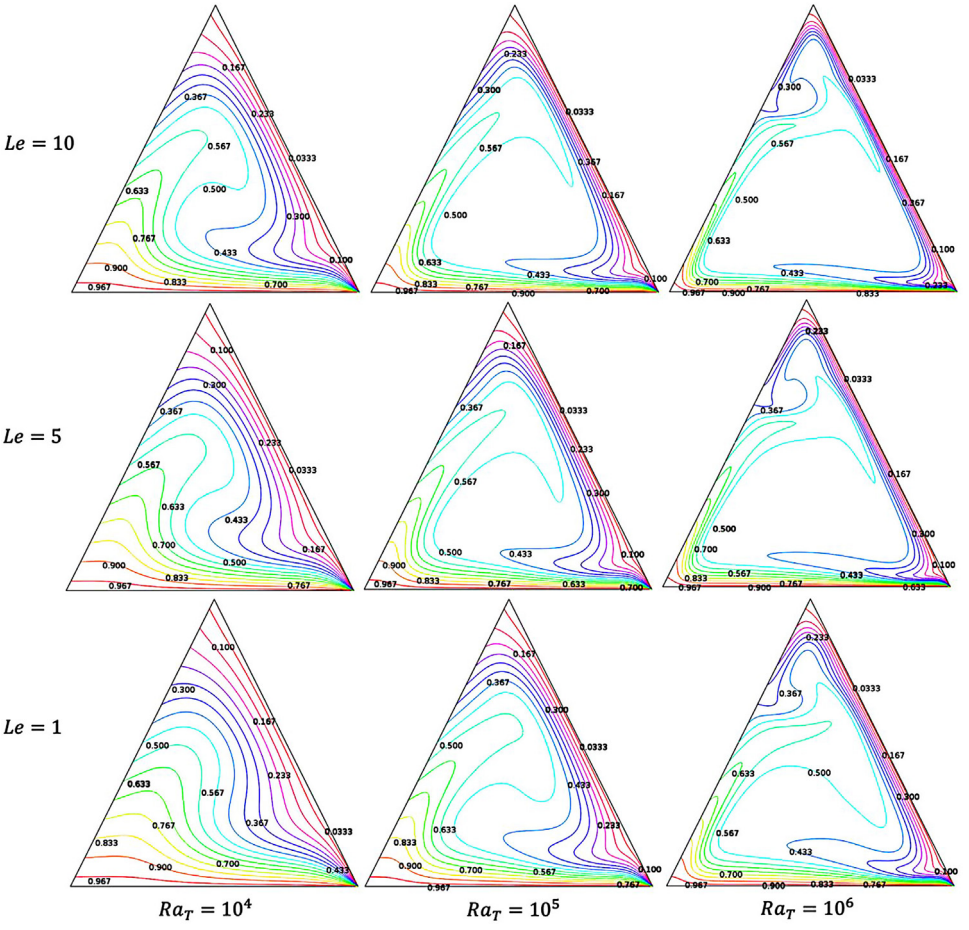

Fig. 8. Isoconcentrations for different values of Ra_T and Le with $Pr = 7.0$, $\varphi = 10\%$, $\lambda = 0$, $N = 1$, $Da = 10^{-3}$.

nanoparticles that can be seen in Fig. 11 (a). When the number of nanoparticles is increased, the solutal boundary layer expands near active walls and thermal boundary layer becomes thinner. For this reason, with the increase of solid volume fraction into the base fluid, heat transfer rate will be enhanced while mass transfer rate will be reduced. From the figure, it can be inferred that both *Nu* and *Sh* are increased considerably when the thermal Rayleigh number is varied from 10^4 to 10^6 and heat and mass transfer rate becomes decrease at $Ra_T = 10^6$.

5. Conclusion

In this study we conducted a numerical simulation to investigate the effect of heat generation, thermal Rayleigh number, solid volume fraction and Lewis number on flow pattern, temperature field and concentration in a triangular cavity filled

http://dx.doi.org/10.1016/j.heliyon.2016.e00140

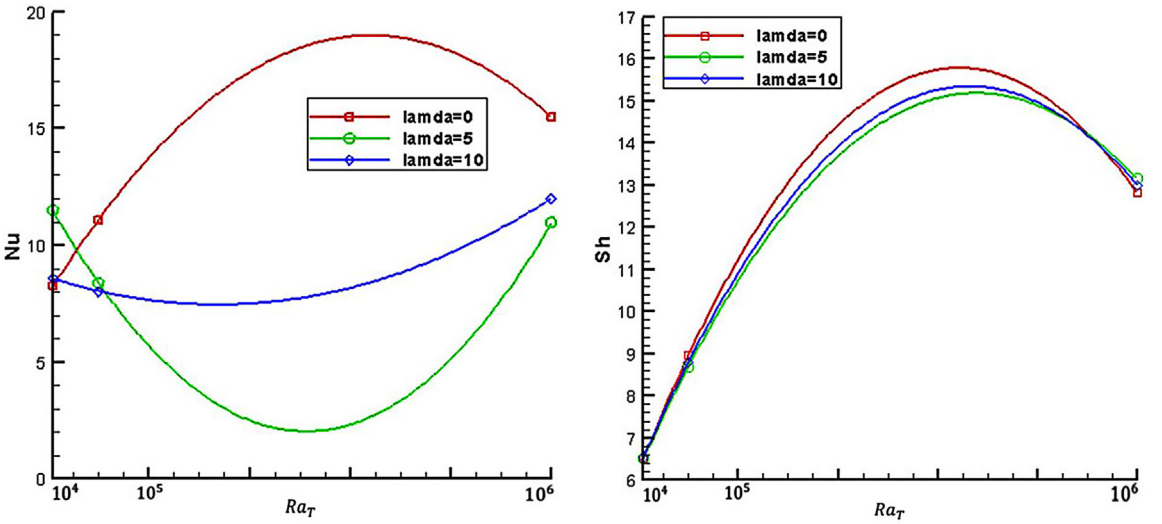

(a) (b)

Fig. 9. The variation of (a) average Nusselt number (*Nu*) and (b) average Sherwood number (*Sh*) along the hot bottom wall for different heat generation parameter and Ra_T with $Pr = 7.0$, $\varphi = 10\%$, $Le = 0$, $N = 1$ and $Da = 10^{-3}$.

porous media saturated Al_2O_3 −water nanofluid. The outcomes of the existing analysis are as follows:

- The heat generation plays an important role on fluid flow pattern, heat and mass transfer.

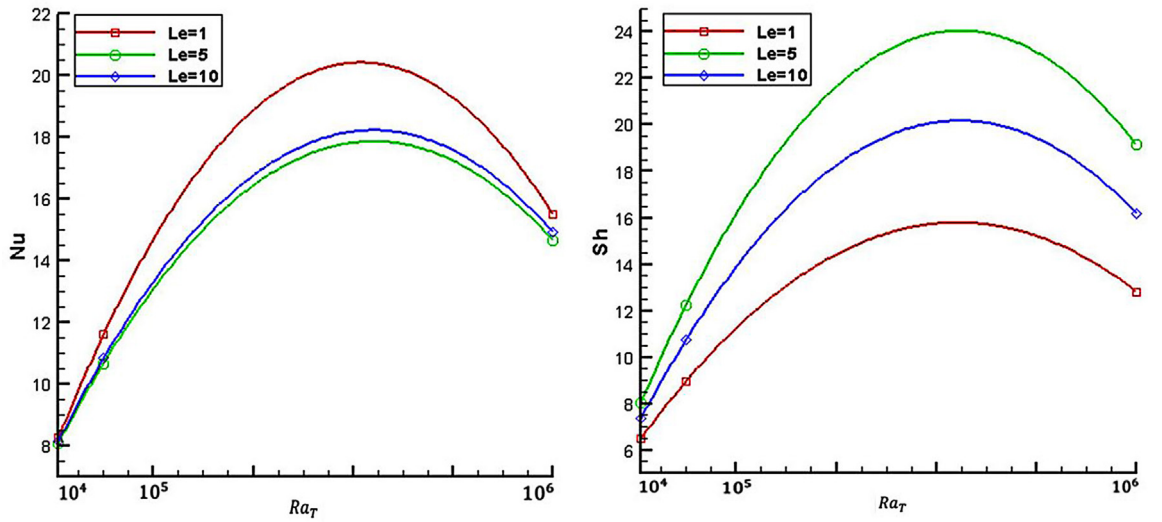

(a) (b)

Fig. 10. The variation of (a) average Nusselt number (*Nu*) and (b) average Sherwood number (*Sh*) along the hot bottom wall for different *Le* and Ra_T with $Pr = 7.0$, $\varphi = 10\%$, $\lambda = 0$, $N = 1$ and $Da = 10^{-3}$.

http://dx.doi.org/10.1016/j.heliyon.2016.e00140

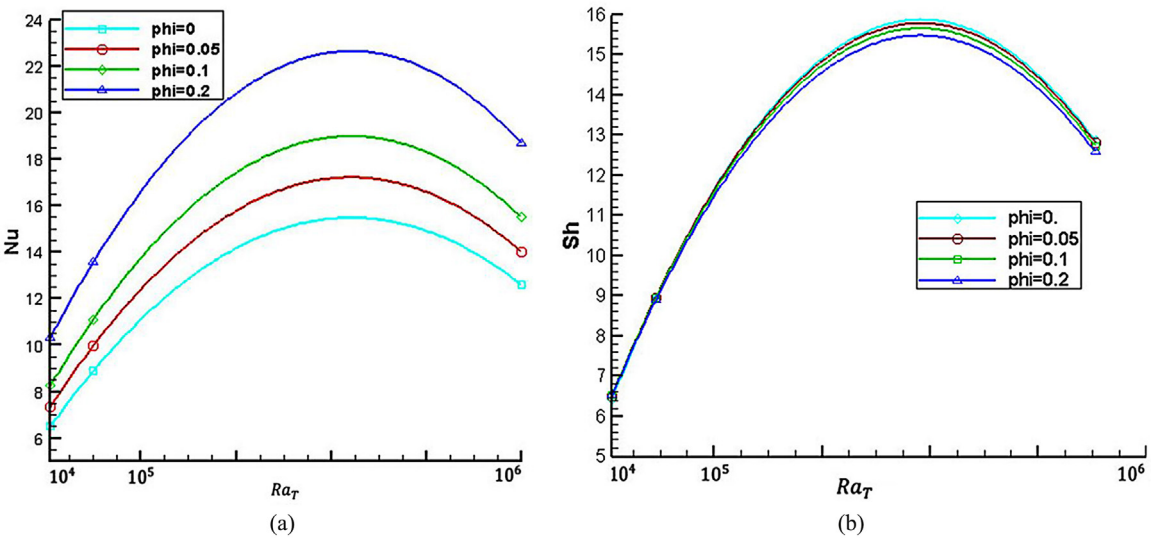

Fig. 11. The variation of (a) average Nusselt number (*Nu*) and (b) average Sherwood number (*Sh*) along the hot bottom wall for different φ and Ra_T with $Pr = 7.0$, $Le = 1$, $\lambda = 0$, $N = 1$ and $Da = 10^{-3}$.

- The flow strength is increased for rising the value of heat generation parameter but decrease for increasing values of Lewis number.
- The average Nusselt number and Sherwood number increases for increasing the Rayleigh number upto $Ra_T = 10^6$ for heat generation parameter, Lewis number and solid volume fraction.
- The rate of heat transfer reduces remarkably with the increasing of heat generation.
- The heat transfer rate increases with the increase of solid volume fraction while the mass transfer rate decreases.

Declarations

Author contribution statement

Raju Chowdhury: Conceived and designed the analysis; Analyzed and interpreted the data; Wrote the paper.

Salma Parvin, Md. Abdul Hakim Khan: Conceived and designed the analysis; Wrote the paper.

Funding statement

This research did not receive any specific grant from funding agencies in the public, commercial, or not-for-profit sectors.

http://dx.doi.org/10.1016/j.heliyon.2016.e00140

Competing interest statement

The authors declare no conflict of interest.

Additional information

No additional information is available for this paper.

References

[1] D.A. Nield, A. Bejan, Convection in Porous Media, 2nd Ed, Springer, New York, 1999.

[2] D.B. Ingham, I. Pop, Transport Phenomena in Porous Media, Pergamon, 1998.

[3] Y. Xuan, Q. Li, Heat transfer enhancement of nanofluids, Int. J. Heat Fluid Flow 21 (2000) 58–64.

[4] N. Putra, W. Roetzel, S.K. Das, Natural convection of nanofluids, Heat Mass Trans. 39 (2003) 775–784.

[5] R.B. Bird, W.E. Stewart, E.N. Lightfoot, Transport phenomena, 2nd Ed., Wiley, New York, 1960.

[6] R. Jou, S. Tzdng, Numerical research of nature convective heat transfer enhancement filled with nanofluids in rectangular enclosure, Int. Commun. Heat Mass Trans. 33 (2006) 727–736.

[7] V. Trisaksri, W. Wongwises, Critical review of heat transfer characteristics of nanofluids, Renewable Sustainable Energy Rev. 11 (2007) 512–523.

[8] A. Abu-Nada, Z. Masoud, A. Hijazi, Natural convection heat transfer enhancement in horizontal concentric annuli using nanofluids, Int. Commun Heat Mass Trans. 35 (2008) 657–665.

[9] K. Khanafer, K. Vafai, M. Lightstone, Buoyancy-driven heat transfer enhancement in a two dimensional enclosure utilizing nanofluids, Int. J. Heat Mass Trans. 46 (2003) 3639–3653.

[10] G.A. Sheikhzadeh, M. Dastmalchi, H. Khoarasanizadeh, Effects of walls temperature variation on double diffusive natural convection of Al_2O_3-water nanofluid in an enclosure, Heat Mass Trans. 49 (2013) 1689–1700.

[11] S. Acharya, R.J. Goldstein, Natural convection in an externally heated vertical or inclined square box containing internal energy sources, J. Heat Trans. 107 (1985) 855–866.

 http://dx.doi.org/10.1016/j.heliyon.2016.e00140

[12] F. Selimefendigil, H.F. Oztop, Natural convection and entropy generation of nanofluid filled cavity having different shaped obstacles under the influence of magnetic field and internal heat generation, J. Tai. Ins. Chem. Eng. 56 (2015) 42–56.

[13] R. Chowdhury, S. Parvin, M.A.H. Khan, A.J. Chamkha, MHD natural convection in a porous equilateral triangular enclosure with a heated square body in the presence of heat generation, Spec. Top. Rev. Porous Med.: Int. J. 6 (2015) 353–365.

[14] F. Selimefendigil, H.F. Oztop, Mixed convection in a two-sided elastic walled and SiO2 nanofluid filled cavity with internal heat generation: Effects of inner rotating cylinder and nanoparticle's shape, J. Mole. Liq. 212 (2015) 509–516.

[15] C. Pang, J.W. Lee, Y.T. Kang, Review on combined heat and mass transfer characteristics in nanofluids, Int. J. Therm. Sci. 87 (2015) 49–67.

[16] O.V. Trevisan, A. Bejan, Combined heat and mass transfer by natural convection in a vertical enclosure, J. Heat Transfer 109 (1987) 104–112.

[17] A. Mojtabi, M.C. Charrier-Mojtabi, Double-diffusive convection in porous media, In: K. Vafai (Ed.), Handbook of Porous Media, Dekker, New York, 2000.

[18] S. Ohtrach, Natural convection with combined driven forces, Physico. Chem. Hydodynamics 1 (1980) 233–247.

[19] R. Viskanta, T.L. Bergman, F.P. Incropera, Double-diffusive natural convection, In: S. Kakac, W. Aung, R. Viskanta (Eds.), Natural Convection: Fundamentals and Applications, Hemisphere, Washington, DC, 1985, pp. 1075–1099.

[20] F. Alavyoon, On natural convection in vertical porous enclosures due to prescribed fluxes of heat and mass at the vertical boundaries, Int. J. Heat Mass Tran. 36 (1993) 2479–2498.

[21] M. Mamou, P. Vasseur, E. Bilgen, D. Gobin, Double diffusive convection in an inclined slot filled with porous medium, European Journal of Mechanics/ Fluids 14 (1995) 629–652.

[22] J.A. Esfahani, V. Bordbar, Double diffusive natural convection heat transfer enhancement in a square enclosure using nanofluids, J. Nanotec. Eng. Medicine 2 (2011) 021002-1–021002-9.

[23] M.A. Teamah, A.F. Elasfty, E.Z. Massoud, Numerical simulation of double diffusive natural convection flow in an inclined rectangular enclosure in the

 http://dx.doi.org/10.1016/j.heliyon.2016.e00140

presence of magnetic field and heat source, Int. J. Therm. Sci. 52 (2012) 161–175.

[24] A. Bejan, Mass and heat transfer by natural convection in a vertical cavity, Int. J. Heat Fluid Flow 6 (1985) 149–159.

[25] Y. Kamotani, L.W. Wang, S. Ostrach, H.D. Jiang, Experimental study of natural convection in shallow enclosures with horizontal temperature and concentration gradients, Int. J. Heat Mass Tran. 28 (1985) 165–173.

[26] M. Mamou, P. Vasseur, E. Bilgen, A Galerkin finite element study of the onset of double-diffusive convection in an inclined porous enclosure, Int. J. Heat Mass Tran 41 (1998) 1513–1529.

[27] R. Chowdhury, S. Parvin, M.A.H. Khan, A.J. Chamkha, Effect of Magnetic Field and Heat Generation on Free Convection in a Porous Media Filled Equilateral Triangular Cavity, Int. J. Eng. Tech. 7 (2015) 49–61.

[28] R.L. Hamilton, O.K. Crosser, Thermal conductivity of heterogeneous two component system, Ind. Eng. Chem. Fund. 1 (1962) 187–191.

[29] H.C. Brinkman, The viscocity of concentrated suspensions and solution, J. Chem. Phys. 20 (1952) 571–581.

[30] S.E. Ahmed, A.M. Rashad, R.S.R. Gorla, Natural Convection in Triangular Enclosures Filled with Nanofluid Saturated Porous Media, J. Therm. Heat Trans. 27 (2013) 700–706.

 http://dx.doi.org/10.1016/j.heliyon.2016.e00140